Science
AAAS

Balancing Volumetric and Gravimetric Uptake in Highly Porous Materials for Clean Energy

Zhijie Chen,[1,⊥] Penghao Li,[1,⊥] Ryther Anderson,[2,⊥] Xingjie Wang,[1] Xuan Zhang,[1] Lee Robison,[1] Louis R. Redfern,[1] Shinya Moribe,[1,6] Timur Islamoglu,[1] Diego A. Gómez-Gualdrón,[2] Taner Yildirim,[3] J. Fraser Stoddart,[1,4,5] and Omar K. Farha[1,7,*]

[1] Department of Chemistry and International Institute of Nanotechnology, Northwestern University, 2145 Sheridan Road, Evanston, Illinois 60208, United States

[2] Department of Chemical and Biological Engineering, Colorado School of Mines, Golden, Colorado 80401, United States

[3] NIST Center for Neutron Research, National Institute of Standards and Technology, Gaithersburg, Maryland 20899, United States

[4] Institute for Molecular Design and Synthesis, Tianjin University, 92 Weijin Road, Tianjin 300072, China

[5] School of Chemistry, University of New South Wales, Sydney, NSW 2052, Australia

[6] Future Mobility Research Department, Toyota Research Institute of North America, Ann Arbor, Michigan 48105, United States

[7] Department of Chemical & Biological Engineering, Northwestern University, 2145 Sheridan Road, Evanston, Illinois 60208, United States

[⊥]These authors contributed equally to this work.

*Corresponding author. Email: o-farha@northwestern.edu

MAIN TEXT

ABSTRACT: A huge challenge facing scientists is the development of adsorbent materials which exhibit ultrahigh porosity but maintain balance between gravimetric and volumetric surface areas for the on-board storage of hydrogen and methane gas—alternatives to conventional fossil fuels. Here we report the simulation-motivated synthesis of ultraporous metal–organic frameworks (MOFs) based on metal trinuclear clusters, namely NU-1501-M (M = Al or Fe). Relative to other ultraporous MOFs, NU-1501-Al exhibits concurrently a high gravimetric Brunauer−Emmett−Teller (BET) area of 7310 m^2 g^{-1} and a volumetric BET area of 2060 m^2 cm^{-3} while satisfying the four BET consistency criteria. The high porosity and surface area of this MOF yielded impressive gravimetric and volumetric storage performances for hydrogen and methane: NU-1501-Al surpasses the gravimetric methane storage DOE target (0.5 g g^{-1}) with a uptake of 0.66 g g^{-1} (262 cm^3 (STP) cm^{-3}) at 100 bar/270 K and a 5−100 bar working capacity of 0.60 g g^{-1} (238 cm^3 (STP) cm^{-3}) at 270 K; and it also shows one of the best deliverable hydrogen capacity (14.0 wt%, 46.2 g L^{-1}) under a combined temperature and pressure swing (77 K/100 bar →160 K/5 bar).

Introduction

In 2017, for the first time in history, the U.S. transportation sector, which includes cars, trucks, planes, trains, and boats, overtook power plants as the largest source of greenhouse gas emissions in the country.(*1*) This progression continued in 2018 as the transportation sector emitted 1.87 billion tons of CO_2 and power plants emitted 1.76 billion tons of CO_2, and this trend is projected to continue.(*1*) This shift in CO_2 emissions makes finding alternative sources of cleaner energy for transportation even more important and judicious.

Methane and hydrogen are both alternatives to gasoline for potential use as fuel for the transportation sector.(*2, 3*) Methane is envisioned as a transitional fuel, as its combustion still emits CO_2, but the amount of CO_2 released is less than gasoline.(*4*) Hydrogen, on the other hand, is envisioned as the "fuel of the future" as hydrogen-powered fuel cell vehicles are zero-emission automobiles.(*2*) However, the transportation, storage, and operations of hydrogen and methane powered vehicles currently require high pressure compression (*i.e.*, 700 bar for H_2 and 250 bar for CH_4), which is both costly and potentially unsafe.(*2, 5*) To encourage research in this important field, the US Department of Energy (DOE) established metrics for the development of on-board storage and delivery systems for alternative fuels for the transportation sector.(*2, 6*) For methane, these targets include a gravimetric storage capacity of 0.5 g g^{-1} and a volumetric storage capacity of 263 cm^3 (STP) cm^{-3}. For hydrogen, these targets (for 2020) include a gravimetric storage capacity of 4.5 wt % and a volumetric storage capacity of 30 g/L.

Developing new adsorbent materials is one of the strategies to reach these targets for the safe and cost-effective storage of methane and hydrogen. In particular, high-surface area porous materials(*3, 7-9*)—often thought of as having a surface area of 2,000 m^2/g or greater—such as metal–organic frameworks (MOFs),(*3, 5, 8, 10-16*) porous carbons,(*5, 17*) covalent organic frameworks(*18*) and porous organic polymers(*19-22*) have been investigated intensively as candidate adsorbents for the on-board storage of clean-energy gases. The properties of these adsorbents could enable gas loadings to power vehicles under less extreme loading pressure (e.g. 100 bar) than that is currently needed by the storage systems used in methane- and hydrogen-powered vehicles. Among these adsorbents, MOFs, constructed from inorganic nodes and organic linkers, have gained prominence as appealing materials for gas storage(*23-27*) due to their tailorable pore chemistry and geometry,

and amenability for rational design facilitated by clear-cut structure-property relationships. Furthermore, surface areas in MOFs have been reported to reach ultrahigh values.(*28-30*)

When using these adsorbents, the tank pressure goes down as fuel is consumed until there is no longer a gradient driving the flow of methane or hydrogen to the engine, which typically occurs at 5 bar.(*2, 26*) At this pressure there may be a significant fraction of gas still adsorbed. Therefore, the deliverable capacity—the amount of stored gas delivered to the engine during operation—becomes a critical design parameter when designing adsorbents. The deliverable capacity for the 100 bar → 5 bar pressure swing has received exceptional interest because 100 bar is the highest refueling pressure for which all-metal Type I pressure tanks can be safety-compliant, circumventing the need for more expensive carbon fiber-reinforced composite vessels for hydrogen storage.(*2, 31*) *As both size and weight requirements for the on-board tank must be met to make the storage system feasible, it is crucial to consider the optimization of volumetric and gravimetric deliverable capacities in MOFs as concurrent objectives rather than separate ones*.(*13, 32-34*)

As the existence of a trade-off between gravimetric and volumetric capacities has become apparent,(*33*) there is a great challenge in providing satisfactory volumetric and gravimetric capacities within a single material. For example, microporous HKUST-1(*5, 35*), with a relatively low gravimetric Brunauer−Emmett−Teller (BET) area of 1980 $m^2\ g^{-1}$ (a volumetric BET area of 1740 $m^2\ cm^{-3}$), exhibits high volumetric storage but moderate gravimetric CH_4 uptake (281 cm^3 (STP) cm^{-3} and 0.23 g g^{-1} at 100 bar/ 298 K), while mesoporous MOF-210(*7*), with a comparatively high gravimetric BET area of 6240 $m^2\ g^{-1}$ (a volumetric BET area of 1560 $m^2\ cm^{-3}$), shows high gravimetric storage capacity yet low volumetric CH_4 uptake (0.48 g g^{-1} and 168 cm^3 (STP) cm^{-3} at 80 bar/ 298 K). Typically, ultraporous MOF materials—*i.e.*, MOF-210(*7*), NU-110(*28*), and DUT-

60(*30*)—with high gravimetric BET areas, though containing high pore volumes and large pore sizes, show relatively low volumetric areas, which limits their applications in gas storage that requires a balance of volumetric and gravimetric capacities. Clearly, one key step toward a satisfactory trade-off between volumetric and gravimetric capacities would be to impart a single material with both high volumetric and gravimetric surface areas.

Results and Discussion

To pursue both high gravimetric and volumetric surface areas in a single material, we used NU-1500(*36*) as a starting point. This class of material has several appealing characteristics, including (i) high porosity and surface area with a relatively small pore size of ~1.4 nm; (ii) a broad degree of designability—the combination of rigid trigonal prismatic linkers and M_3O metal trimers will form MOFs with the **acs** net; (iii) good moisture stability for ease of processing; (iv) and finally the versality of metal trimers allow it to be synthesized from M^{3+} metals, including abundant metals such as aluminum and iron. To start, we synthesized a new aluminum MOF, NU-1500-Al—$[Al_3(\mu_3\text{-}O)(H_2O)_2(OH)(PET)]$, which exhibits 6-c **acs** topology and has rigid trigonal prismatic triptycene-based organic ligands—*i.e.*, peripherally extended triptycene(*37*) (H_6PET)—and aluminum μ_3-oxo-centred trinuclear clusters(*38*) (**Fig. S5 and S10**). We confirmed the permanent microporosity of activated NU-1500-Al by nitrogen (N_2) adsorption isotherm at 77 K, which exhibited an apparent BET area of 3560 $m^2\ g^{-1}$—satisfying the four BET consistency criteria(*39, 40*)—and which also had an experimental total pore volume of 1.46 $cm^3\ g^{-1}$, in good agreement with the value for the simulated structure and previously reported(*36*) NU-1500-Fe (**Figs. S15-17**). The volumetric BET area of NU-1500-Al is estimated to be ~1770 $m^2\ cm^{-3}$, based on the crystallographic density from the simulated structure. The pore-size distribution from a density

functional theory (DFT) model with slit pore geometry revealed one type of pore centered at 1.4 nm, which agrees with the previous values from other NU-1500 analogues(*36*) (**Fig. S19**).

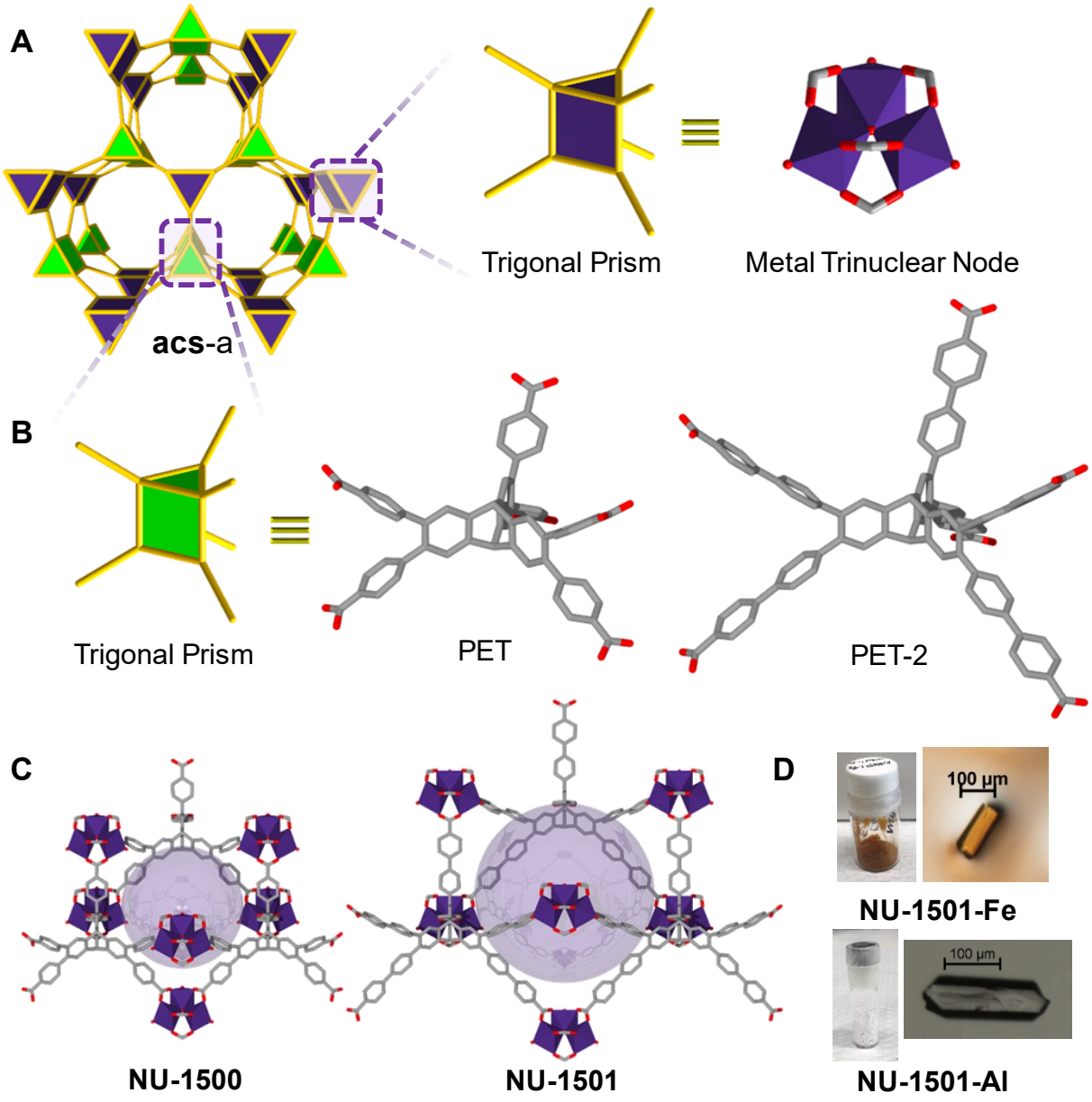

Fig. 1. (A-C) Schematic representation of **NU-1501-M** (M = Fe and Al) with the 6-c **acs** net. Atom color scheme: C, grey; metal, polyhedron with Northwestern University (NU) purple; O, red. H atoms are omitted for the sake of clarity. (D) Optical images of the single crystals of NU-1501.

On account of its high micropore volume and surface area, high-pressure H_2 and CH_4 sorption studies were conducted on NU-1500-Al at the National Institute for Standards and Technology (NIST) (**Figs. S31-36**). At 100 bar, NU-1500-Al adsorbed ~0.34 g g^{-1} (237 cm^3 (STP) cm^{-3}) and ~0.39 g g^{-1} (273 cm^3 (STP) cm^{-3}) of CH_4 at 296 K and 270 K, respectively, with deliverable capacities of 0.29 g g^{-1} (202 cm^3 (STP) cm^{-3}) and ~0.32 g g^{-1} (224 cm^3 (STP) cm^{-3}) between 5 bar and 100 bar. The volumetric deliverable capacities of 5−100 bar for NU-1500-Al are comparable to those of benchmark methane storage materials, such as MOF-905(*25*) (203 cm^3 (STP) cm^{-3}; 5−80 bar at 298 K), HKUST-1(*5*) (207 cm^3 (STP) cm^{-3}; 5−100 bar at 298 K), and Al-**soc**-MOF-1(*13*) (201 cm^3 (STP) cm^{-3}; 5−80 bar at 298 K) (**Table S6**). NU-1500-Al adsorbed ~8.6 wt% (46.8 g L^{-1}) of H_2 at 100 bar and 77 K, with a deliverable capacity of 8.2 wt% (44.6 g L^{-1}) under combined temperature and pressure swing condition: 77 K/100 bar →160 K/5 bar, which agrees with the tank design conditions proposed(*41*) by the DOE (**Table S7**).

Motivated by the results from NU-1500, we first set out to understand the trade-off between gravimetric and volumetric surface area (GSA and VSA, respectively). To accomplish this, a topologically diverse (58 topologies) 2800-MOF database, including 50 isoreticular MOFs to NU-1500, was created using the ToBaCCo(*42*) code (**Figs. S50-54**). Both gravimetric and volumetric surface areas were calculated geometrically for the created structures. Plotting these two quantities against each other (**Fig. 2A**) reveals their tradeoff, which can be quantified by their *normalized* product (GSA x VSA).

The GSA x VSA product show a volcano-type relationship between MOF helium void fraction (VF) and largest pore diameter (LPD) (**Fig. 2B, C**), with MOFs at the top of the volcano presenting the ideal trade-off (GSA x VSA product in the 95th percentile). The intermediate MOFs in this database that still exhibit these ideal qualities display an average VF of 0.85 and an average LPD

of 17.2 Å. By comparison, NU-1500 presents values of 0.76 and 12.7 Å, respectively, indicating opportunities to improve the tradeoff by refining the MOF design. Indeed, the obtained structure-property relationships revealed the value of extending the rigid triptycene-based ligand of the NU-1500 by one phenyl ring, going from PET to PET-2(*43*) (**Fig. 1**).

We coined the PET-2-based structure as NU-1501 and noticed that it presents properties (VF = 0.87, LPD = 18.8 Å) closer to the average of the MOFs in the ideal trade-off region. Note that simply meeting either property value does not guarantee an ideal tradeoff. For instance, MOFs with "ideal" VF cover a wide range for the GSA x VSA product. Thus, NU-1501 has other complementary features that boost its GSA x VSA product such as low metal to organic atom ratio. For example, **Figs. S51E** and **51F** show that MOFs with lower metal atom to organic atom ratios tend to have higher GSA × VSA, which is simply because organic atom moieties (e.g. aromatic rings) tend to provide large adsorption surfaces while being light compared to metals.

To understand the implications of an ideal VSA vs GSA trade-off, we predicted methane and hydrogen deliverable capacities for the MOFs in the database (**Fig. 2E, F**). Notably, there is broader peak in the gravimetric deliverable capacity (GDC) vs. volumetric deliverable capacity (VDC) than in the VSA vs. GSA tradeoff, meaning that MOFs with maximally high GDC (and thus generally maximally high GSA) are included in the ideal tradeoff region. From **Fig. S54** we see that there are many MOFs within the ideal tradeoff region for deliverable capacity that have too high a GSA to be in the ideal tradeoff region for surface area. NU-1501 lies exactly at the boundary of MOFs in the ideal tradeoff region for deliverable capacity and MOFs in the ideal tradeoff region for surface area (in all cases), meaning that NU-1501-Al maintains maximally high VSA for MOFs with GDC × VDC in the 95th percentile (most others having higher GSA and lower VSA).

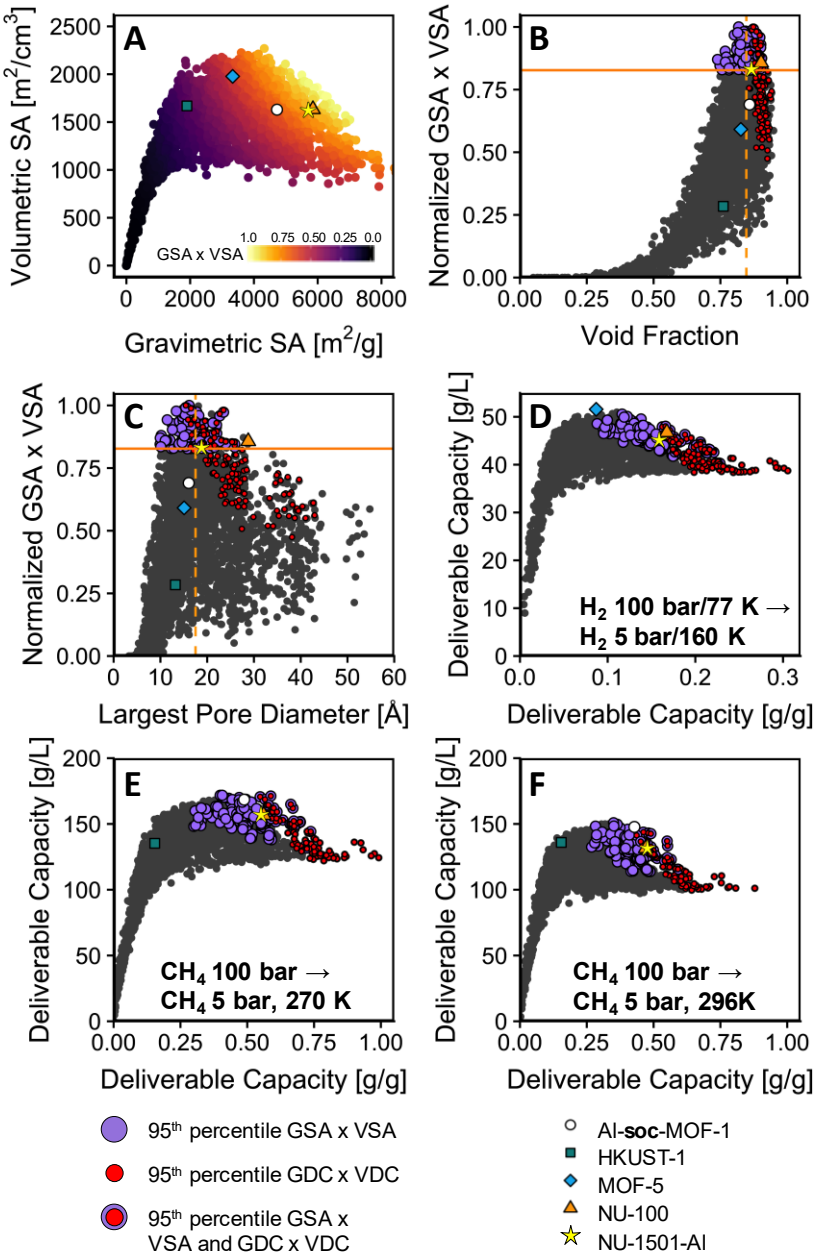

Fig. 2. (A) Volumetric SA vs. gravimetric SA, colored by the product of the two. NU-1501-Al lies in the ideal tradeoff region, characterized as being just past the peak of volumetric SA. Al-**soc**-MOF-1, HKUST-1, MOF-5, and NU-100 are shown as a comparison. (B) The product of GSA and VSA verses void fraction. The orange line shows the cutoff for being in the 95th percentile of GSA x VSA. The dashed, orange line shows the average void fraction for MOFs in the 95th percentile.

(C) Analogous to B) except plotting GSA x VSA versus MOF largest pore diameter. (D) Volumetric deliverable capacity (VDC) vs. gravimetric deliverable capacity (GDC) for hydrogen. Purple points show MOFs in the ideal region (95th percentile of GSA x VSA) of the GSA/VSA tradeoff. Red points show MOFs in the 95th percentile of GDC x VDC. Red points outlined in purple show MOFs in both regions. (E) Analogous to D) expect for methane VDC and GDC at 270 K. (F) Analogous to D) except for methane VDC and GDC at 296 K.

Inspired by the computational results above, we decided to synthesize expanded versions of **acs**-MOFs—*i.e.*, NU-1501 which feature an extended ligand design, H_6PET-2 (**Figs. S1-4**)). Solvothermal reactions of H_6PET-2 with $AlCl_3 \cdot 6H_2O$ and $FeCl_3 \cdot 6H_2O$ yielded (**Fig. 1D**) colorless and yellow-orange hexagonal block crystals. Single-crystal X-ray diffraction (SCXRD) studies of these materials (NU-1501-Al and NU-1501-Fe) revealed non-catenated structures crystallizing in a hexagonal space group (*P*-6*m*2) (**Tables S1-2**). The μ_3-oxo-centred trinuclear metal inorganic clusters are linked by the fully deprotonated trigonal prismatic ligands, H_6PET-2, to yield a 3-periodic **acs**-MOF having one type of open hexagonal channels with a pore size of ~2.2 nm. We predicted the formula to be $[M_3(\mu_3\text{-}O)(H_2O)_2(OH)(\text{PET-2})]$ (M = Al or Fe), with the terminal anionic groups on the trinuclear node being -OH, as supported by the absence of chloride signals from EDS analysis (**Figs. S11-13**). We confirmed the phase purities of the bulk NU-1501-Al and NU-1501-Fe based on similarities (**Fig. S6**) between the simulated and as-synthesized PXRD patterns.

The permanent porosity of NU-1501-Al and NU-1501-Fe after supercritical CO_2 activation have been confirmed by reversible N_2 and Ar adsorption and desorption isotherms at 77 K and 87 K, respectively. Both materials have very similar isotherms (**Fig. 3** and **Figs. S18-24)**. The experimental total pore volumes of NU-1501-Al, calculated from the N_2 and Ar adsorption

isotherms, are 2.91 and 2.93 $cm^3\ g^{-1}$, respectively, which agree well with the simulated values from the single crystal structure. The pore-size distribution based on a DFT model revealed that NU-1501-Al has pore sizes ranging from 1.5 to 2.5 nm, with two types of pores centered at ~1.7 and 2.2 nm, which agrees well with the two pores from the single crystal structure. The apparent BET area of NU-1501-Al based on the N_2 adsorption isotherm is estimated to be 7310 $m^2\ g^{-1}$ after satisfying all four BET consistency criteria.(*39, 40*) If only the first two BET consistency criteria are fulfilled—as in the recently reported(*30*) ultraporous material, DUT-60—the apparent BET area is estimated to reach 9150 $m^2\ g^{-1}$ (**Table S3**). Moreover, the apparent BET area of NU-1501-Al, based on the Ar adsorption isotherm attains 7920 $m^2\ g^{-1}$ after satisfying the first three BET consistency criteria, which is in line with the simulated BET area of 7760 $m^2\ g^{-1}$ from the simulated Ar adsorption isotherm (**Table S4**). It should be noted that the deviation from the BET criteria should be minimized when it is not possible to select a region fulfilling all four consistency criteria, as in the case of the BET area calculation(*40*) from the Ar adsorption isotherm of NU-1501-Al. To the best of our knowledge, the gravimetric BET area (7310 $m^2\ g^{-1}$) of NU-1501-Al is the highest reported value for all porous materials after satisfying all four BET criteria, despite the pore volume (about 2.90 $cm^3\ g^{-1}$) being lower than those of ultraporous materials having BET areas larger than 7000 $m^2\ g^{-1}$ (**Table S5**). Remarkably, the volumetric BET area of NU-1501-Al reaches 2060 $m^2\ cm^{-3}$ based on the crystallographic density. This BET area is among the highest of all reported porous materials with BET areas higher than 5000 $m^2\ g^{-1}$, and is much higher than that of similar ultraporous MOFs such as NU-110(*28*) (1585 $m^2\ cm^{-3}$), MOF-210(*7*) (1560 $m^2\ cm^{-3}$), and DUT-60(*30*) (1466 $m^2\ cm^{-3}$). Importantly, the isotherm is highly reproducible, as illustrated by the similarities of isotherms taken from four different batches at Northwestern University and at NIST (**Fig. S18**).

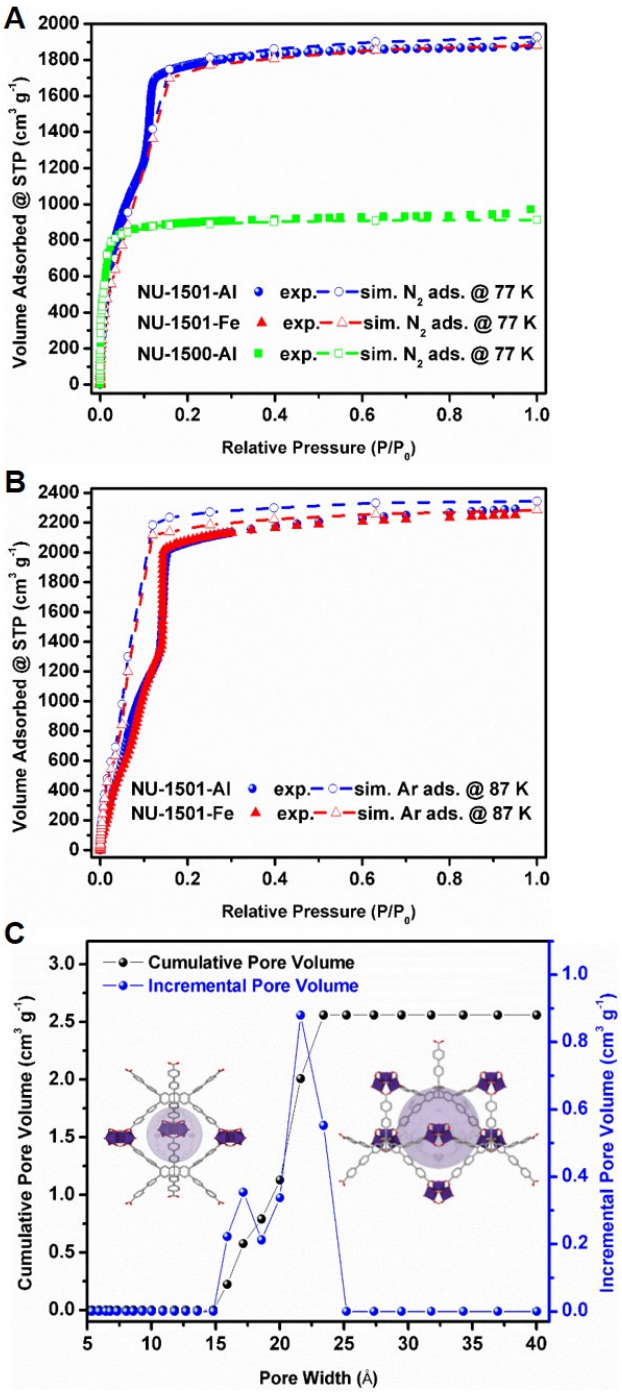

Fig. 3. (A) Experimental and simulated N_2 (77 K) adsorption isotherms of NU-1501 and NU-1500-Al. (B) Experimental and simulated Ar (87 K) adsorption isotherms of NU-1501. (C) DFT pore size distribution of NU-1501-Al from N_2 (77 K) adsorption isotherm. The dashed lines are used to guide the eyes for simulated data.

As revealed by the geometrical calculation of the pore size distribution from the crystal structures (**Fig. S49**), there are two main features that allow NU-1501-Al to maintain a higher volumetric surface area over other MOFs—*i.e.*, MOF-210(*7*), NU-100(*8*), NU-110(*28*), and DUT-60(*30*)—with similar gravimetric surface areas and higher pore volumes: (i) the largest pore of NU-1501-Al is much smaller than those of MOF-210(*7*), NU-100(*8*), NU-110(*28*), and DUT-60(*30*) and (ii) NU-1501-Al has only one dominant pore.

The iron-based analogue of NU-1501 (NU-1501-Fe) shows similar gravimetric and volumetric BET areas (7140 m^2 g^{-1} and 2130 m^2 cm^{-3}) as the aluminum-based NU-1501 and also features similarly sized experimental pore volume (2.90 cm^3 g^{-1}) as NU-1501-Al, illustrating the versatility of this MOF design and synthetic strategy (**Fig. S20**). Molecular simulations further revealed that NU-1501-Al and NU-1501-Fe have higher geometric surface areas (5714 and 5513 m^2 g^{-1}, respectively) calculated with the N_2 probe than that of NU-1500-Al (3634 m^2 g^{-1}) (**Table S8**). Additionally, the trivalent metal-based trimer (*i.e.*, Al_3O or Fe_3O) of NU-1501 produces a relatively more stable framework than the traditional ultraporous MOFs with BET areas larger than 6000 m^2 g^{-1} based on Zn_4O or copper paddlewheel building units.(*7, 28, 30, 36*) The overall stability of NU-1501 was tested via SCXRD, PXRD and N_2 sorption measurements after soaking in liquid water, and variable temperature PXRD studies (**Table S2 and Figs. S7-9, 14, 25-27**). To this end, NU-1501 represents an ultraporous material balancing both gravimetric and volumetric BET areas simultaneously—*i.e.*, larger than 7000 m^2 g^{-1} and 2000 m^2 cm^{-3}—making them promising candidates for clean energy related gas storage (*i.e.*, H_2 and CH_4).

Considering the exceptional gravimetric and volumetric surface areas, methane and hydrogen high-pressure sorption experiments were performed on activated NU-1501 at NIST (**Fig. 4** and **Figs. S37-48**). NU-1501-Al displays one of the top gravimetric methane uptakes among MOF

materials at 80 bar—0.60 g g^{-1} at 270 K and 0.48 g g^{-1} at 296 K. The 5-80 bar methane working capacities of NU-1501-Al are 0.44 g g^{-1} (174 cm^3 (STP) cm^{-3}; 296 K) and ~0.54 g g^{-1} (214 cm^3 (STP) cm^{-3}; 270 K). These methane capacities are comparable to those of other MOF materials such as MOF-210(*7*), Al-**soc**-MOF-1(*13*), ST-2(*44*) and MOF-905(*25*). At room temperature, the gravimetric deliverable methane capacity of NU-1501-Al at working pressure between 80 bar (adsorption) and 5 bar (desorption) is comparatively similar to that of the benchmark Al-**soc**-MOF-1 while the volumetric deliverable capacity is slightly lower (**Fig. 5**). Notably, NU-1501-Al adsorbed ~0.54 g g^{-1} (214 cm^3 (STP) cm^{-3}) and ~0.66 g g^{-1} (262 cm^3 (STP) cm^{-3}) of CH_4 at 100 bar and at 296 K and 270 K, respectively. Deliverable capacities between 5 bar and 100 bar are 0.50 g g^{-1} (198 cm^3 (STP) cm^{-3}; 296 K) and ~0.60 g g^{-1} (238 cm^3 (STP) cm^{-3}; 270 K), suggesting NU-1501-Al is among the best porous crystalline materials for methane storage (**Table S6**). The uptake capacities of NU-1501-Al surpass the materials-level gravimetric CH_4 storage DOE target (0.5 g g^{-1}) at 100 bar at both room temperature and 270 K.(*6, 9, 25*) The gravimetric deliverable capacity at 270 K and 5-100 bar—*i.e.*, 0.60 g g^{-1}—is even higher than that of the recently reported record MOF materials (**Table S6**). The gravimetric methane uptakes at 100 bar at 296 K and 270 K are also much higher than those of the microporous isostructural NU-1500-Al (0.34 g g^{-1} at 296K and 0.39 g g^{-1} at 270 K; at 100 bar), despite similar volumetric uptake (214 vs. 237 cm^3 (STP) cm^{-3} at 296 K; 262 vs. 273 cm^3 (STP) cm^{-3} at 270 K). This suggests the isoreticular extension of NU-1500 to NU-1501 significantly increases gravimetric methane capacity without sacrificing volumetric performance. Additionally, at near freezing temperatures, NU-1501-Al shows **(Fig. 5F)** a higher volumetric 5-100 bar deliverable methane capacity than HKUST-1 (238 cm^3 (STP) cm^{-3} at 270 K vs. 195 cm^3 (STP) cm^{-3} at 273 K) due to the much lower unused methane uptake at 5 bar while having a considerably better gravimetric 5-100 bar deliverable capacity (0.60 g g^{-1} at 270 K

vs. 0.16 g g^{-1} at 273 K). NU-1501-Fe, compared to NU-1501-Al, adsorbed slightly less CH_4 (~0.52 g g^{-1} at 296 K and ~0.63 g g^{-1} at 270 K; at 100 bar) under the same conditions due to the slightly lower surface area and pore volume (**Figs. S45-48**).

The isosteric heats of adsorption (Q_{st}) of NU-1501-Al for CH_4 (**Figs. S42**) were calculated from the isotherms and found to be 9.7 and 10.9 kJ mol^{-1} at low and high loading, respectively. The experimental Q_{st} of NU-1501-Al is close to the enthalpy of adsorption calculated from Monte Carlo simulations in the grand canonical ensemble (GCMC) simulations at low pressure—10.3 kJ mol^{-1} (**Table S9**). This data suggests moderate host−guest interactions occur between the framework and methane gas, which is ideal for achieving high deliverable capacities. The Q_{st} value of NU-1501 is slightly less than NU-1500-Al (13.7 kJ mol^{-1}) and is most likely due to smaller pore size of NU-1500. The simulated adsorption isotherms at various temperatures and pressures closely resemble the experimental isotherms, further validating the successful activation of the materials and the high-pressure adsorption results of NU-1501.

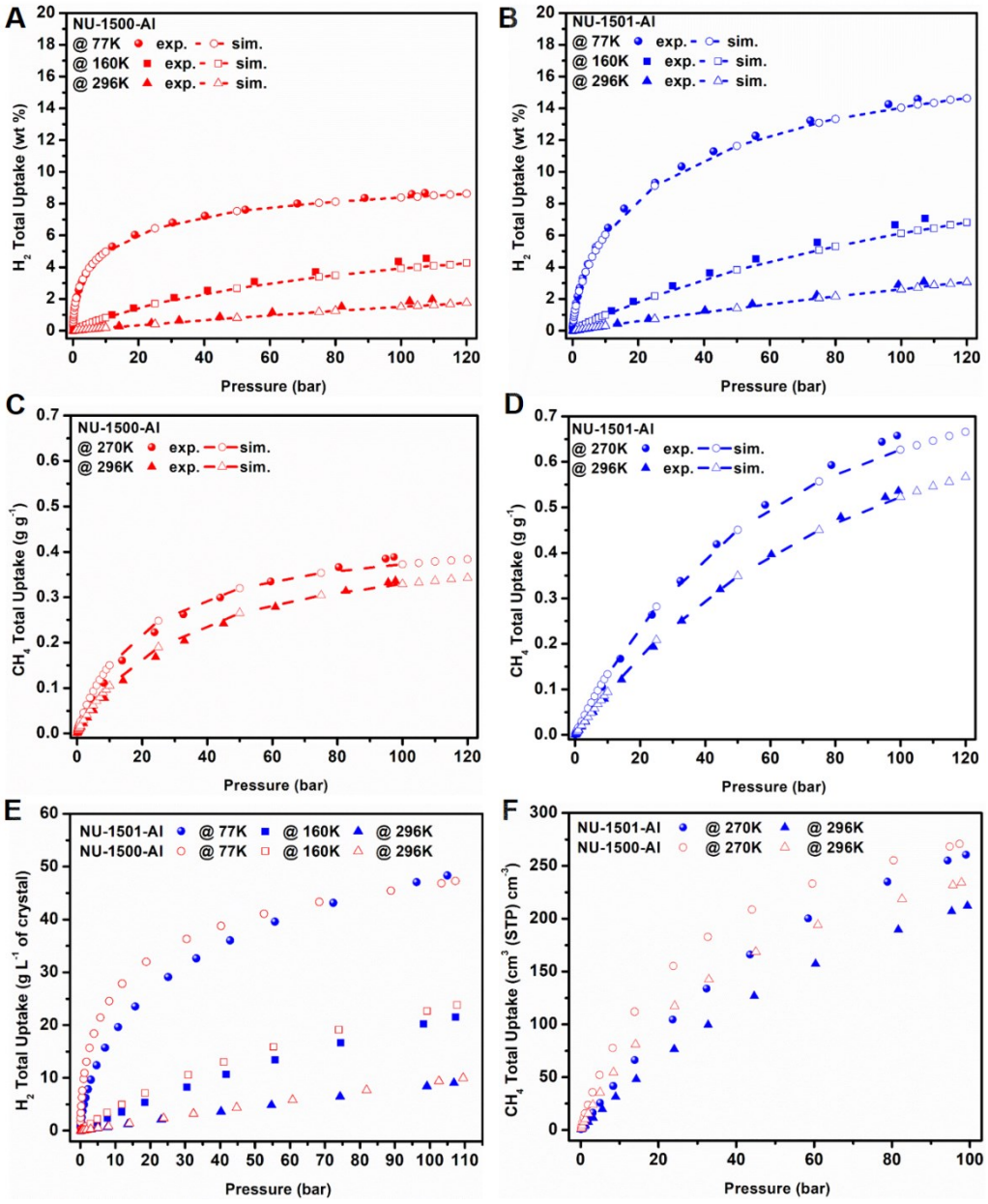

Fig. 4. (A-B) Experimental and simulated hydrogen adsorption uptake for NU-1501-Al and NU-1500-Al at 77 K, 160 K and 296 K. (C-D) Experimental and simulated methane adsorption uptake for NU-1501-Al and NU-1500-Al at 270 K and 296 K. In this work, the capacity (in wt%) of H_2 is calculated according to wt% = (mass of H_2)/(mass of H_2 + mass of MOF) × 100%. The dashed lines are used to guide the eyes for simulated data. (E-F) Volumetric adsorption uptake of hydrogen and methane for NU-1501-Al and NU-1500-Al, calculated based on crystallographic density.

Remarkably, NU-1501-Al and NU-1501-Fe are among the best MOFs for hydrogen storage under combined temperature and pressure swing conditions (77 K/100 bar →160 K/5 bar) (**Fig. 5B** and **Table S7**).(*33, 34, 41, 45*) H_2 adsorption isotherms revealed NU-1501-Al adsorbs ~14.5 wt% (47.9 g L^{-1}) of H_2 at 100 bar and 77 K, with a high deliverable capacity of 14.0 wt% (46.2 g L^{-1}) under the conditions: 77 K/100 bar →160 K/5 bar. NU-1501-Fe shows a slightly lower deliverable capacity (13.2 wt%; 45.4 g L^{-1}) than NU-1501-Al under the same conditions. The experimental H_2 adsorption isotherms closely match the simulated isotherms at various temperatures, which confirmed the near complete activation of the MOFs. In addition, both the absolute uptake at 100 bar/ 77 K and the deliverable capacities of NU-1501-Al for H_2 are much higher than those of NU-1500-Al while maintaining nearly identical volumetric uptake and capacities (14.0 wt% vs. 8.2 wt% and 46.2 g L^{-1} vs. 44.6 g L^{-1} under the aforementioned operational condition), further demonstrating the effectiveness of extension of this **acs**-MOF platform in balancing the gravimetric and volumetric performance of H_2 storage. In agreement with the simulated results, the experimental gravimetric uptake of H_2 for NU-1501-Al at 100 bar and 296 K is ~2.9 wt% (volumetric uptake: 8.4 g L^{-1}) far exceeds the values of reported MOFs (generally between 1−2 wt % at 100 bar at room temperature).(*11, 12, 46*)

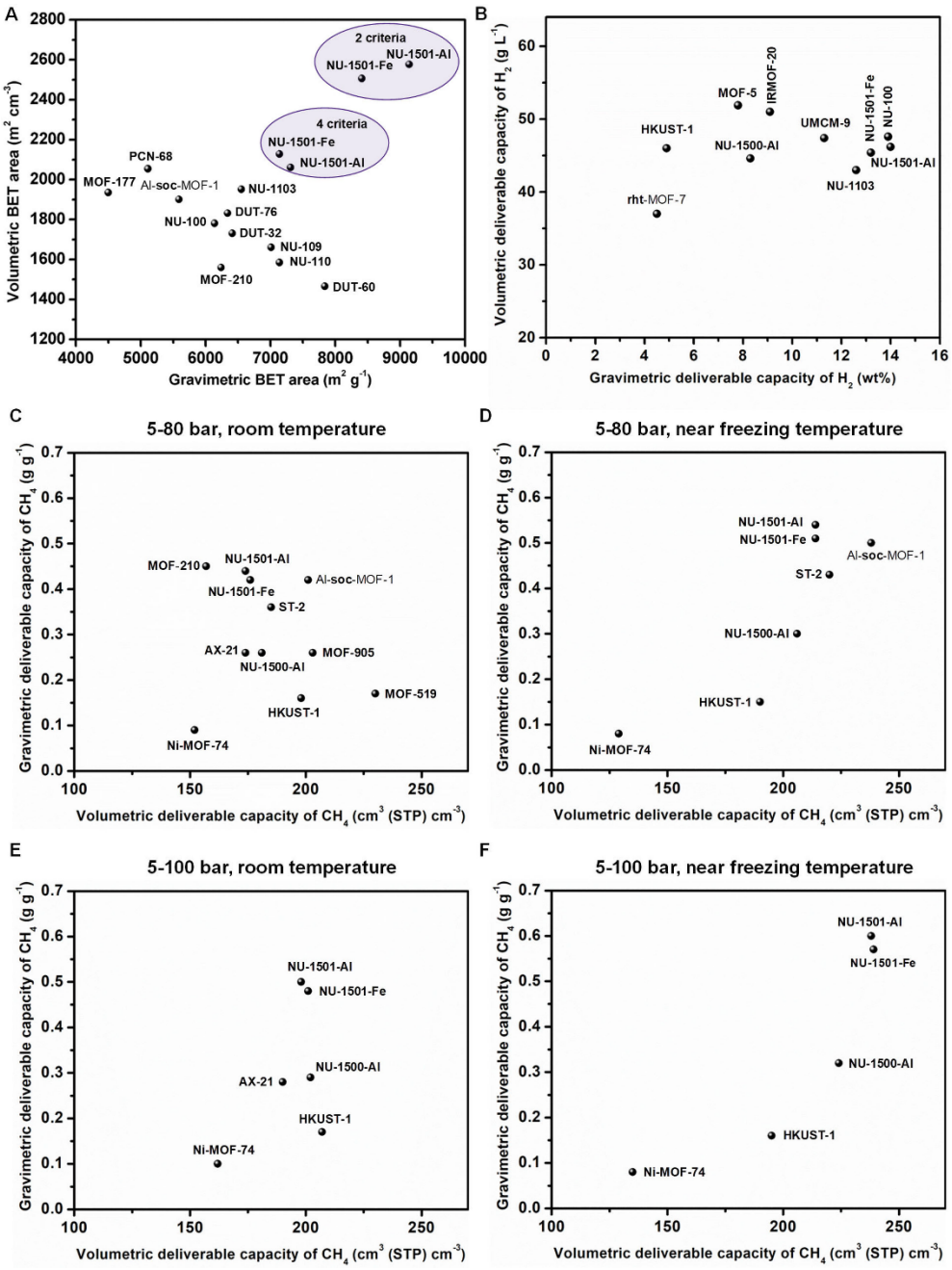

Fig. 5. (A) Trade-off between gravimetric and volumetric BET area for selected ultrahigh porous materials. (B) Trade-off between gravimetric and volumetric deliverable hydrogen capacity under combined temperature and pressure swing condition: 77 K/100 bar →160 K/5 bar. (C-F) Trade-off between gravimetric and volumetric deliverable methane capacity of MOFs for 5−80 bar and 5−100 bar at room temperature and near freezing temperature. Methane adsorption isotherms of

MOFs in this work are performed at 296 K and 270 K, and methane adsorption isotherms of other materials for comparison are performed at 298 K and 273 K. For details of comparison, see **Tables S6-7** and **Fig. S28-30**.

Additionally, the Q_{st} values from the H_2 adsorption isotherms at various temperatures indicated NU-1501-Al exhibits small Q_{st} values of 4 and 2.6 kJ mol^{-1} at low and high loading, respectively. The Q_{st} for H_2 of NU-1501 at low loading is close to the enthalpy of adsorption from GCMC simulations at low pressure and slightly less than the Q_{st} of NU-1500-Al—*i.e.*, 4.9 kJ mol^{-1} (**Table S9**). These values indicate the MOFs have modest host−guest interactions and that the large hydrogen capacities observed experimentally is driven by adsorbate−adsorbate interactions and the frameworks' substantial porosities. The combination of the experimentally obtained high-pressure hydrogen adsorption studies and GCMC molecular simulations demonstrate that the NU-1501 series are promising candidate materials for the on-board storage of hydrogen gas due to their ultrahigh gravimetric and volumetric surface areas and moderate pore volumes of ~2.90 cm^3 g^{-1} (in comparison to traditional ultraporous MOFs) and balance both volumetric and gravimetric capacity.

Conclusions

In conclusion we have rationally designed and synthesized a class of ultraporous MOFs, NU-1501, with narrow mesoporosity and which exhibit pore diameters less than 2.5 nm. These MOFs balance both the gravimetric and volumetric BET areas, which make them ideal candidates for new adsorbent materials for the safe and effective storage of methane and hydrogen gas for on-board storage tanks. Particularly, NU-1501 has the highest apparent gravimetric BET areas among porous materials after satisfying all four BET consistency criteria. With a moderate pore volume compared to the conventional ultraporous materials such as MOF-210(*7*), NU-110(*28*), and DUT-

60(*30*), NU-1501 exhibits impressive volumetric BET areas. The combination of experiment and molecular simulation reveals that NU-1501 achieves outstanding gravimetric uptake, volumetric uptake, and delivery capacities of methane and hydrogen simultaneously under practical operational conditions, making these materials a novel class of promising MOF adsorbent candidates for the storage and delivery of methane and hydrogen—clean energy carriers related to the carbon-neutral energy system. Finally, the unambiguous structure-property relationship derived from the performance of this material, high-throughput computational modeling, and experimental results will fuel the design and synthesis of the next-generation of ultraporous sorbents for storage and delivery of clean fuel sources.

References

1. *U.S. Energy Information Administration (EIA), Monthly Energy Review, DOE/EIA - 0035(2019/7), July 2019*.
2. M. D. Allendorf *et al.*, An assessment of strategies for the development of solid-state adsorbents for vehicular hydrogen storage. *Energy Environ. Sci.* **11**, 2784-2812 (2018). doi: 10.1039/C8EE01085D
3. A. Schoedel, Z. Ji, O. M. Yaghi, The role of metal–organic frameworks in a carbon-neutral energy cycle. *Nat. Energy* **1**, 16034 (2016). doi: 10.1038/nenergy.2016.34
4. *U.S. Energy Information Administration (EIA), Carbon Dioxide Emissions Coefficients (https://www.eia.gov/environment/emissions/co2_vol_mass.php), release date: February 2, 2016.*
5. J. A. Mason, M. Veenstra, J. R. Long, Evaluating metal-organic frameworks for natural gas storage. *Chem. Sci.* **5**, 32-51 (2014). doi: 10.1039/C3SC52633J
6. Y. Peng *et al.*, Methane Storage in Metal–Organic Frameworks: Current Records, Surprise Findings, and Challenges. *J. Am. Chem. Soc.* **135**, 11887-11894 (2013). doi: 10.1021/ja4045289
7. H. Furukawa *et al.*, Ultrahigh Porosity in Metal-Organic Frameworks. *Science* **329**, 424-428 (2010). doi: 10.1126/science.1192160
8. O. K. Farha *et al.*, De novo synthesis of a metal–organic framework material featuring ultrahigh surface area and gas storage capacities. *Nat. Chem.* **2**, 944-948 (2010). doi: 10.1038/nchem.834
9. B. Li, H.-M. Wen, W. Zhou, Jeff Q. Xu, B. Chen, Porous Metal-Organic Frameworks: Promising Materials for Methane Storage. *Chem* **1**, 557-580 (2016). doi: 10.1016/j.chempr.2016.09.009

10. M. Eddaoudi *et al.*, Systematic design of pore size and functionality in isoreticular MOFs and their application in methane storage. *Science* **295**, 469-472 (2002). doi: 10.1126/science.1067208
11. D. Zhao, D. Yuan, H.-C. Zhou, The current status of hydrogen storage in metal–organic frameworks. *Energy Environ. Sci.* **1**, 222-235 (2008). doi: 10.1039/B808322N
12. M. P. Suh, H. J. Park, T. K. Prasad, D.-W. Lim, Hydrogen Storage in Metal–Organic Frameworks. *Chem. Rev.* **112**, 782-835 (2012). doi: 10.1021/cr200274s
13. D. Alezi *et al.*, MOF Crystal Chemistry Paving the Way to Gas Storage Needs: Aluminum-Based soc-MOF for CH_4, O_2, and CO_2 Storage. *J. Am. Chem. Soc.* **137**, 13308-13318 (2015). doi: 10.1021/jacs.5b07053
14. M. T. Kapelewski *et al.*, Record High Hydrogen Storage Capacity in the Metal–Organic Framework Ni_2(m-dobdc) at Near-Ambient Temperatures. *Chem. Mater.* **30**, 8179-8189 (2018). doi: 10.1021/acs.chemmater.8b03276
15. T. Tian *et al.*, A sol–gel monolithic metal–organic framework with enhanced methane uptake. *Nat. Mater* **17**, 174 (2017). doi: 10.1038/nmat5050
16. Y. Yan, S. Yang, A. J. Blake, M. Schröder, Studies on Metal–Organic Frameworks of Cu(II) with Isophthalate Linkers for Hydrogen Storage. *Acc. Chem. Res.* **47**, 296-307 (2013). doi: 10.1021/ar400049h
17. K. V. Kumar, K. Preuss, M.-M. Titirici, F. Rodríguez-Reinoso, Nanoporous Materials for the Onboard Storage of Natural Gas. *Chem. Rev.* **117**, 1796-1825 (2017). doi: 10.1021/acs.chemrev.6b00505
18. H. Furukawa, O. M. Yaghi, Storage of Hydrogen, Methane, and Carbon Dioxide in Highly Porous Covalent Organic Frameworks for Clean Energy Applications. *J. Am. Chem. Soc.* **131**, 8875-8883 (2009). doi: 10.1021/ja9015765
19. D. Yuan, W. Lu, D. Zhao, H.-C. Zhou, Highly Stable Porous Polymer Networks with Exceptionally High Gas-Uptake Capacities. *Adv. Mater.* **23**, 3723-3725 (2011). doi: 10.1002/adma.201101759
20. J. Jia *et al.*, Extremely Hydrophobic POPs to Access Highly Porous Storage Media and Capturing Agent for Organic Vapors. *Chem* **5**, 180-191 (2019). doi: 10.1016/j.chempr.2018.10.005
21. C. D. Wood *et al.*, Hydrogen Storage in Microporous Hypercrosslinked Organic Polymer Networks. *Chem. Mater.* **19**, 2034-2048 (2007). doi: 10.1021/cm070356a
22. V. Rozyyev *et al.*, High-capacity methane storage in flexible alkane-linked porous aromatic network polymers. *Nat. Energy* **4**, 604-611 (2019). doi: 10.1038/s41560-019-0427-x
23. S. i. Noro, S. Kitagawa, M. Kondo, K. Seki, A New, Methane Adsorbent, Porous Coordination Polymer [{$CuSiF_6$(4,4′-bipyridine)$_2$}$_n$]. *Angew. Chem. Int. Ed.* **39**, 2081-2084 (2000). doi: 10.1002/1521-3773(20000616)39:12<2081::AID-ANIE2081>3.0.CO;2-A
24. P. L. Llewellyn *et al.*, High Uptakes of CO_2 and CH_4 in Mesoporous Metal—Organic Frameworks MIL-100 and MIL-101. *Langmuir* **24**, 7245-7250 (2008). doi: 10.1021/la800227x
25. J. Jiang, H. Furukawa, Y.-B. Zhang, O. M. Yaghi, High Methane Storage Working Capacity in Metal–Organic Frameworks with Acrylate Links. *J. Am. Chem. Soc.* **138**, 10244-10251 (2016). doi: 10.1021/jacs.6b05261

26. F. Gándara, H. Furukawa, S. Lee, O. M. Yaghi, High Methane Storage Capacity in Aluminum Metal–Organic Frameworks. *J. Am. Chem. Soc.* **136**, 5271-5274 (2014). doi: 10.1021/ja501606h
27. R. Grünker *et al.*, A new metal–organic framework with ultra-high surface area. *Chem. Commun.* **50**, 3450-3452 (2014). doi: 10.1039/C4CC00113C
28. O. K. Farha *et al.*, Metal–Organic Framework Materials with Ultrahigh Surface Areas: Is the Sky the Limit? *J. Am. Chem. Soc.* **134**, 15016-15021 (2012). doi: 10.1021/ja3055639
29. S. B. Kalidindi *et al.*, Chemical and Structural Stability of Zirconium-based Metal–Organic Frameworks with Large Three-Dimensional Pores by Linker Engineering. *Angew. Chem. Int. Ed.* **54**, 221-226 (2015). doi: 10.1002/anie.201406501
30. I. M. Honicke *et al.*, Balancing Mechanical Stability and Ultrahigh Porosity in Crystalline Framework Materials. *Angew. Chem. Int. Ed.* **57**, 13780-13783 (2018). doi: 10.1002/anie.201808240
31. D. J. Durbin, C. Malardier-Jugroot, Review of hydrogen storage techniques for on board vehicle applications. *Int. J. Hydrogen Energy* **38**, 14595-14617 (2013). doi: 10.1016/j.ijhydene.2013.07.058
32. Y. Peng *et al.*, Simultaneously high gravimetric and volumetric methane uptake characteristics of the metal–organic framework NU-111. *Chem. Commun.* **49**, 2992-2994 (2013). doi: 10.1039/C3CC40819A
33. D. A. Gómez-Gualdrón *et al.*, Understanding Volumetric and Gravimetric Hydrogen Adsorption Trade-off in Metal–Organic Frameworks. *ACS Appl. Mater. Interfaces* **9**, 33419-33428 (2017). doi: 10.1021/acsami.7b01190
34. A. Ahmed *et al.*, Balancing gravimetric and volumetric hydrogen density in MOFs. *Energy Environ. Sci.* **10**, 2459-2471 (2017). doi: 10.1039/C7EE02477K
35. S. S.-Y. Chui, S. M.-F. Lo, J. P. H. Charmant, A. G. Orpen, I. D. Williams, A Chemically Functionalizable Nanoporous Material $[Cu_3(TMA)_2(H_2O)_3]$. *Science* **283**, 1148-1150 (1999). doi: 10.1126/science.283.5405.1148
36. Z. Chen *et al.*, Reticular Access to Highly Porous acs-MOFs with Rigid Trigonal Prismatic Linkers for Water Sorption. *J. Am. Chem. Soc.* **141**, 2900-2905 (2019). doi: 10.1021/jacs.8b13710
37. P. Li *et al.*, Interpenetration Isomerism in Triptycene-Based Hydrogen-Bonded Organic Frameworks. *Angew. Chem. Int. Ed.* **58**, 1664-1669 (2019). doi: 10.1002/anie.201811263
38. T. Devic, C. Serre, High valence 3p and transition metal based MOFs. *Chem. Soc. Rev.* **43**, 6097-6115 (2014). doi: 10.1039/C4CS00081A
39. J. L. Rouquerol, P.; Rouquerol, F., P. L. R.-R. Llewellyn, F.; Rouquerol, J.; Seaton, N., Eds, Ed. (Elsevier, Amsterdam, 2007), vol. 160, pp. 49.
40. D. A. Gómez-Gualdrón, P. Z. Moghadam, J. T. Hupp, O. K. Farha, R. Q. Snurr, Application of Consistency Criteria To Calculate BET Areas of Micro- And Mesoporous Metal–Organic Frameworks. *J. Am. Chem. Soc.* **138**, 215-224 (2016). doi: 10.1021/jacs.5b10266
41. P. García-Holley *et al.*, Benchmark Study of Hydrogen Storage in Metal–Organic Frameworks under Temperature and Pressure Swing Conditions. *ACS Energy Lett.* **3**, 748-754 (2018). doi: 10.1021/acsenergylett.8b00154
42. Y. J. Colón, D. A. Gómez-Gualdrón, R. Q. Snurr, Topologically Guided, Automated Construction of Metal–Organic Frameworks and Their Evaluation for Energy-Related Applications. *Cryst. Growth Des.* **17**, 5801-5810 (2017). doi: 10.1021/acs.cgd.7b00848

43. Z. Chen *et al.*, Ligand-Directed Reticular Synthesis of Catalytically Active Missing Zirconium-Based Metal–Organic Frameworks. *J. Am. Chem. Soc.* **141**, 12229-12235 (2019). doi: 10.1021/jacs.9b06179
44. C.-C. Liang *et al.*, Engineering of Pore Geometry for Ultrahigh Capacity Methane Storage in Mesoporous Metal–Organic Frameworks. *J. Am. Chem. Soc.* **139**, 13300-13303 (2017). doi: 10.1021/jacs.7b08347
45. A. Ahmed *et al.*, Exceptional hydrogen storage achieved by screening nearly half a million metal-organic frameworks. *Nat. Commun* **10**, 1568 (2019). doi: 10.1038/s41467-019-09365-w
46. K. Sumida, M. R. Hill, S. Horike, A. Dailly, J. R. Long, Synthesis and Hydrogen Storage Properties of $Be_{12}(OH)_{12}$(1,3,5-benzenetribenzoate)$_4$. *J. Am. Chem. Soc.* **131**, 15120-15121 (2009). doi: 10.1021/ja9072707
47. B. J. Bucior *et al.*, Identification Schemes for Metal–Organic Frameworks To Enable Rapid Search and Cheminformatics Analysis. *Cryst. Growth Des.* **19**, 6682-6697 (2019). doi: 10.1021/acs.cgd.9b01050
48. P. Kissel, D. J. Murray, W. J. Wulftange, V. J. Catalano, B. T. King, A nanoporous two-dimensional polymer by single-crystal-to-single-crystal photopolymerization. *Nat. Chem.* **6**, 774 (2014). doi: 10.1038/nchem.2008
49. S. Vela *et al.*, Determining the Attenuation Factor in Molecular Wires Featuring Covalent and Noncovalent Tectons. *Angew. Chem. Int. Ed.* **55**, 15076-15080 (2016). doi: 10.1002/anie.201608973
50. N. C. Bruno, M. T. Tudge, S. L. Buchwald, Design and preparation of new palladium precatalysts for C–C and C–N cross-coupling reactions. *Chem. Sci.* **4**, 916-920 (2013). doi: 10.1039/C2SC20903A
51. G. Sheldrick, SHELXT - Integrated space-group and crystal-structure determination. *Acta Cryst. A* **71**, 3-8 (2015). doi: 10.1107/S2053273314026370
52. G. Sheldrick, Crystal structure refinement with SHELXL. *Acta Cryst. C* **71**, 3-8 (2015). doi: 10.1107/S2053229614024218
53. O. V. Dolomanov, L. J. Bourhis, R. J. Gildea, J. A. K. Howard, H. Puschmann, OLEX2: a complete structure solution, refinement and analysis program. *J. Appl. Cryst.* **42**, 339-341 (2009). doi: 10.1107/S0021889808042726
54. A. Spek, Structure validation in chemical crystallography. *Acta Cryst. D* **65**, 148-155 (2009). doi: 10.1107/S090744490804362X
55. A. P. Nelson, O. K. Farha, K. L. Mulfort, J. T. Hupp, Supercritical Processing as a Route to High Internal Surface Areas and Permanent Microporosity in Metal−Organic Framework Materials. *J. Am. Chem. Soc.* **131**, 458-460 (2009). doi: 10.1021/ja808853q
56. W. Zhou, H. Wu, M. R. Hartman, T. Yildirim, Hydrogen and Methane Adsorption in Metal−Organic Frameworks: A High-Pressure Volumetric Study. *J. Phys. Chem. C* **111**, 16131-16137 (2007). doi: 10.1021/jp074889i
57. J. Jagiello, T. J. Bandosz, K. Putyera, J. A. Schwarz, Adsorption near Ambient Temperatures of Methane, Carbon Tetrafluoride, and Sulfur Hexafluoride on Commercial Activated Carbons. *J. Chem. Eng. Data.* **40**, 1288-1292 (1995). doi: 10.1021/je00022a033
58. J. Jagiełło, T. J. Bandosz, J. A. Schwarz, Characterization of Microporous Carbons Using Adsorption at Near Ambient Temperatures. *Langmuir* **12**, 2837-2842 (1996). doi: 10.1021/la960093r

59. D. Dubbeldam, S. Calero, D. E. Ellis, R. Q. Snurr, RASPA: molecular simulation software for adsorption and diffusion in flexible nanoporous materials. *Mol. Simul.* **42**, 81-101 (2016). doi: 10.1080/08927022.2015.1010082
60. S. L. Mayo, B. D. Olafson, W. A. Goddard, DREIDING: a generic force field for molecular simulations. *J. Phys. Chem.* **94**, 8897-8909 (1990). doi: 10.1021/j100389a010
61. J. J. Potoff, J. I. Siepmann, Vapor–liquid equilibria of mixtures containing alkanes, carbon dioxide, and nitrogen. *AIChE J.* **47**, 1676-1682 (2001). doi: 10.1002/aic.690470719
62. M. G. Martin, J. I. Siepmann, Transferable Potentials for Phase Equilibria. 1. United-Atom Description of n-Alkanes. *J. Phys. Chem. B* **102**, 2569-2577 (1998). doi: 10.1021/jp972543+
63. D. A. Gomez-Gualdron *et al.*, Evaluating topologically diverse metal-organic frameworks for cryo-adsorbed hydrogen storage. *Energy Environ. Sci.* **9**, 3279-3289 (2016). doi: 10.1039/C6EE02104B
64. G. Anderson, B. Schweitzer, R. Anderson, D. A. Gómez-Gualdrón, Attainable Volumetric Targets for Adsorption-Based Hydrogen Storage in Porous Crystals: Molecular Simulation and Machine Learning. *J. Phys. Chem. C* **123**, 120-130 (2019). doi: 10.1021/acs.jpcc.8b09420
65. D. Levesque, A. Gicquel, F. L. Darkrim, S. B. Kayiran, Monte Carlo simulations of hydrogen storage in carbon nanotubes. *J. Phys. Condens. Matter* **14**, 9285-9293 (2002). doi: 10.1088/0953-8984/14/40/318
66. D. P. Nicholson, N. G. , *Computer Simulation and the Statistical Mechanics of Adsorption*. (London, 1982).
67. A. Torres-Knoop, A. Poursaeidesfahani, T. J. H. Vlugt, D. Dubbeldam, Behavior of the Enthalpy of Adsorption in Nanoporous Materials Close to Saturation Conditions. *J. Chem. Theory Comput.* **13**, 3326-3339 (2017). doi: 10.1021/acs.jctc.6b01193
68. R. Anderson, D. A. Gómez-Gualdrón, Increasing topological diversity during computational "synthesis" of porous crystals: how and why. *CrystEngComm* **21**, 1653-1665 (2019). doi: 10.1039/C8CE01637B
69. S. Plimpton, Fast Parallel Algorithms for Short-Range Molecular Dynamics. *Journal of Computational Physics* **117**, 1-19 (1995). doi: 10.1006/jcph.1995.1039
70. A. K. Rappe, C. J. Casewit, K. S. Colwell, W. A. Goddard, W. M. Skiff, UFF, a full periodic table force field for molecular mechanics and molecular dynamics simulations. *J. Am. Chem. Soc.* **114**, 10024-10035 (1992). doi: 10.1021/ja00051a040
71. N. Klein *et al.*, A Mesoporous Metal–Organic Framework. *Angew. Chem. Int. Ed.* **48**, 9954-9957 (2009). doi: 10.1002/anie.200904599
72. K. Koh, A. G. Wong-Foy, A. J. Matzger, A Porous Coordination Copolymer with over 5000 m2/g BET Surface Area. *J. Am. Chem. Soc.* **131**, 4184-4185 (2009). doi: 10.1021/ja809985t
73. L. D. Gelb, K. E. Gubbins, Pore Size Distributions in Porous Glasses: A Computer Simulation Study. *Langmuir* **15**, 305-308 (1999). doi: 10.1021/la9808418
74. P. Llewellyn, G. Maurin, J. Rouquerol, in *Adsorption by Powders and Porous Solids (Second Edition)*. (Academic Press, Oxford, 2014), pp. 565-610.
75. H. Li, M. Eddaoudi, M. O'Keeffe, O. M. Yaghi, Design and synthesis of an exceptionally stable and highly porous metal-organic framework. *Nature* **402**, 276-279 (1999). doi: 10.1038/46248

76. S. S. Kaye, A. Dailly, O. M. Yaghi, J. R. Long, Impact of Preparation and Handling on the Hydrogen Storage Properties of Zn4O(1,4-benzenedicarboxylate)3 (MOF-5). *J. Am. Chem. Soc.* **129**, 14176-14177 (2007). doi: 10.1021/ja076877g
77. G. Férey *et al.*, A Chromium Terephthalate-Based Solid with Unusually Large Pore Volumes and Surface Area. *Science* **309**, 2040-2042 (2005). doi: 10.1126/science.1116275
78. J. An *et al.*, Metal-adeninate vertices for the construction of an exceptionally porous metal-organic framework. *Nat. Commun* **3**, 604 (2012). doi: 10.1038/ncomms1618
79. H. Furukawa, M. A. Miller, O. M. Yaghi, Independent verification of the saturation hydrogen uptake in MOF-177 and establishment of a benchmark for hydrogen adsorption in metal–organic frameworks. *J. Mater. Chem.* **17**, 3197-3204 (2007). doi: 10.1039/B703608F
80. D. Yuan, D. Zhao, D. Sun, H.-C. Zhou, An Isoreticular Series of Metal–Organic Frameworks with Dendritic Hexacarboxylate Ligands and Exceptionally High Gas-Uptake Capacity. *Angew. Chem. Int. Ed.* **49**, 5357-5361 (2010). doi: 10.1002/anie.201001009
81. U. Stoeck, I. Senkovska, V. Bon, S. Krause, S. Kaskel, Assembly of metal-organic polyhedra into highly porous frameworks for ethene delivery. *Chem. Commun.* **51**, 1046-1049 (2015). doi: 10.1039/C4CC07920E
82. T. C. Wang *et al.*, Ultrahigh Surface Area Zirconium MOFs and Insights into the Applicability of the BET Theory. *J. Am. Chem. Soc.* **137**, 3585-3591 (2015). doi: 10.1021/ja512973b
83. B. Li *et al.*, A Porous Metal–Organic Framework with Dynamic Pyrimidine Groups Exhibiting Record High Methane Storage Working Capacity. *J. Am. Chem. Soc.* **136**, 6207-6210 (2014). doi: 10.1021/ja501810r

Acknowledgement

Funding: O.K.F. gratefully acknowledges research support from the U.S. Department of Energy's Office of Energy Efficiency and Renewable Energy (EERE) under the award number DE-EE0008816. P.L. and J.F.S. acknowledge the Joint Center of Excellence in Integrated Nano-Systems (JCIN) at King Abdulaziz City for Science and Technology (KACST) and Northwestern University (NU). D.A.G-G. acknowledges funding from NSF CAREER (award CBET 1846707). Simulations were performed at the Mio supercomputer cluster maintained by the Colorado School of Mines. L.R.'s contribution to this work is based on work supported by the U.S. Department of Energy (DOE), Office of Science, Office of Workforce Development for Teachers and Scientists, Office of Science Graduate Student Research (SCGSR) program. The SCGSR program is

administered by the Oak Ridge Institute for Science and Education (ORISE) for the DOE. ORISE is managed by ORAU under contract DE-SC0014664. This work made use of the EPIC facility of Northwestern University's NU*ANCE* Center, which has received support from the Soft and Hybrid Nanotechnology Experimental (SHyNE) Resource (NSF ECCS-1542205); the MRSEC program (NSF DMR-1720139) at the Materials Research Center; the International Institute for Nanotechnology (IIN); the Keck Foundation; and the State of Illinois, through the IIN. This work made use of the IMSERC at Northwestern University, which has received support from the Soft and Hybrid Nanotechnology Experimental (SHyNE) Resource (NSF ECCS-1542205), the State of Illinois, and the International Institute for Nanotechnology (IIN). **Authors contributions:** O.K.F. supervised the project; Z.C. and O.K.F. conceived and designed the experiments; P.L. synthesized the ligand under the supervision of J.F.S.; Z.C. synthesized MOF materials; R.A. conducted molecular simulation under the supervision of D.A.G.; X.W. and Z.C. performed activation and low-pressure sorption in Northwestern University; Z.C. collected and analyzed the single crystal data with the help from X.Z.; Z.C. characterized MOF materials with the help from X.W., L.R., L.R.R., S.M. and T.I.; T.Y. conducted the low-pressure and high-pressure sorption studies at NIST with the samples sent from Northwestern University; Z.C. analyzed low-pressure and high-pressure sorption data with the help from O.K.F., R.A., D.A.G., and T.Y.; Z.C., L.R., and O.K.F. wrote the manuscript and all authors commented and revised on the manuscript. **Competing interests:** O.K.F. have financial interest in NuMat Technologies, a startup company that is seeking to commercialize MOFs. **Data and materials availability:** The X-ray crystallographic data for NU-1501-Al and NU-1501-Fe have been deposited at the Cambridge Crystallographic Data Centre (CCDC), under deposition number CCDC 1909853, 1909854, and 1945113. These data can be obtained free of charge from the CCDC via www.ccdc.cam.ac.uk.

Crystallographic information for NU-1501-Al and NU-1501-Fe can also be found in Supplementary Data. MOFkey(*47*): Al.PZUNVLJATCTESM.MOFkey-v1.acs (NU-1500-Al), Fe.GKGWJFNTVGTMJR.MOFkey-v1.acs (NU-1501-Fe), Al.GKGWJFNTVGTMJR.MOFkey-v1.acs (NU-1501-Al). All other relevant data supporting the findings of this study are presented in the paper or the Supplementary Materials.

SUPPLEMENTARY MATERIALS

Materials and Methods
Supplementary Text
Figs. S1 to S54
Tables S1 to S10
Captions for Data S1 to S3
References (48-83)
Data S1 to S3